Environmental Geology (1995) 26: 157–165

K. Y. Lee · C. V. Chrysikopoulos

Numerical modeling of three-dimensional contaminant migration from dissolution of multicomponent NAPL pools in saturated porous media

Received: 27 January 1995/ Accepted: 10 April 1995

Abstract A three-dimensional model for contaminant transport resulting from the dissolution of multicomponent nonaqueous phase liquid (NAPL) pools in three-dimensional saturated subsurface formations is developed. The solution is obtained numerically by a finite-difference scheme, and it is suitable for homogeneous porous media with unidirectional interstitial velocity. Each dissolved component may undergo first-order decay and may sorb under local equilibrium conditions. It is also assumed that the dissolution process is mass transfer limited. The nonaqueous phase activity coefficients of the NAPL pool components are evaluated at each time step. The model behavior is illustrated through a synthetic example with a NAPL pool consisting of a mixture of TCA (1,1,2-trichloroethane) and TCE (trichloroethylene). The numerical solution presented in this work is in good agreement with a recently developed analytical solution for the special case of a single component NAPL pool. The results indicate the importance of accounting for the necessary changes in the organic phase activity which significantly affects the equilibrium aqueous solubility.

Key words Multicomponent NAPL · Contaminant transport · Dissolution · Numerical simulation

Introduction

Leaking underground gas tanks, hazardous waste dump sites, industrial waste outlets, and accidental land spills are just a few possible sources of man-made groundwater contamination. As the number of contaminated sites around the world increases, people are getting more aware of the environmental impact that groundwater contamination has on present and future generations. In particular, nonaqueous phase liquids (NAPLs) are the focus of many studies. Environmental engineers are especially concerned with the quality of groundwater once these NAPLs penatrate into subsurface formations. A small amount of a NAPL can be a long-lasting source of groundwater contamination due to its slow dissolution rate (Anderson and others 1992a, Johnson and Pankow 1992). Therefore, it is necessary and essential for environmental engineers to model and predict the contaminant transport resulting from the dissolution of NAPLs in the subsurface.

As NAPLs migrate through the unsaturated zone, ganglia are formed from residual segments of NAPL breaking off from the main body of the liquid and are held in aquifer pore spaces by capillary forces (Geller and Hunt 1993). Once the main body of the liquid reaches the groundwater table, solvents with densities lower than water create a concentrated pool at the top of the groundwater table (floaters or LNAPLs), whereas solvents with densities heavier than water keep on migrating down the saturated zone and create a concentrated pool when they reach an impermeable layer (sinkers or DNAPLs). As time goes on, solutes from these NAPL pools are transported, slowly creating plumes of contamination in the direction of the groundwater movement.

The majority of the studies available in the literature focus on the migration of NAPLs and dissolution of residual segments (Pinder and Abriola 1986; Hunt and others 1988; Geller 1990; Miller and others 1990; Powers and others 1991, 1992; Adenekan and others 1993). The literature on NAPL pool dissolution is rather limited. Only the studies by Hunt and others (1988), Anderson and others (1992b), Whelan (1992), Voudrias and Yeh (1994), Chrysikopoulos and others (1994), and Chrysikopoulos (1995) have investigated the dissolution from NAPL pools.

Anderson and others (1992b) conducted several dissolution experiments with pools of dense chlorinated hydrocarbon (CHC) solvents. They concluded that saturation concentration can be achieved rapidly near the vicinity of an immobile organic fluid; and at typical groundwater velocities, dissolution times for CHC pools containing a few hundred to a few thousand kilograms of solvent range

K. Y. Lee · C. V. Chrysikopoulos (✉)
Department of Civil and Environmental Engineering, University of California, Irvine, California 92717-2175, USA

from decades to centuries. Whelan (1992) conducted a multicomponent DNAPL pool dissolution experiment using a mixture of TCA and TCE. Voudrias and Yeh (1994) performed dissolution experiments with a toluene pool floating at the water table under constant and variable hydraulic gradients. They concluded that pulsed pumping is more efficient than continuous pumping for remediation of contaminated aquifers. Chrysikopoulos and others (1994) conducted dissolution experiments with trichloroethylene pools and presented a two-dimensional analytical model that simulated the experimental data quite well. Chrysikopoulos (1995) presented analytical models of single component stagnant pool dissolution for both rectangular and elliptic pools and demonstrated through synthetic examples that the more elongated the pool along the direction of the interstitial flow, the higher the dissolved peak concentration.

For multicomponent NAPL systems, the dissolution rate is controlled in part by the equilibrium aqueous solubility of each individual component (Banerjee 1984; Borden and Piwoni 1992). The aqueous solubility is described by a relationship that equates the activities in the nonaqueous (organic) and aqueous phases and is a function of the time-dependent mole fraction of each component. As the mole fraction of each component changes constantly with a rate proportional to its mass transfer coefficient, the activity coefficient of each component is also changing accordingly (Fredenslund and others 1977). It should be noted that the activity coefficient is a dimensionless correction term indicating the nonideality of the solution (Stumm and Morgan 1981). The higher the activity coefficient, the greater the degree of nonideality of a solution. Banerjee (1984) demonstrated experimentally that for a NAPL mixture containing components of similar structure, the organic phase activity coefficients can be approximated at ideal state equal to one, and the equilibrium aqueous solubility is a function of mole fraction only.

For multicomponent NAPL mixtures with components of dissimilar structure, the organic phase activity coefficient can be estimated using the software UNIFAC (UNI-Functional group Activity Coefficients; Fredenslund and others 1977). The program UNIFAC was initially developed for chemical engineering applications associated with activity coefficient estimations in organic mixtures where limited or no experimental data are available. The activity coefficient estimation is based on the group-contribution method, which consists of a combinatorial part and a residual part. By considering each molecule as the sum of the functioning groups that constitute that molecule (e.g., methylene, nitro, keto, amino, carboxyl), the combinatorial part accounts for the size and shape of the molecules present in the organic mixture while the residual part accounts for energy interactions among the different functioning groups. The thermodynamic properties of a solution are then estimated according to the functioning groups that comprise the mixture. Finally, UNIFAC uses the information about the functioning groups to calculate the activity coefficient for each molecule.

In this work, the governing coupled partial differential equations describing the multicomponent NAPL dissolution problem in conjunction with the appropriate boundary conditions are solved numerically by a finite-difference scheme. A synthetic example with a multicomponent NAPL pool consisting of a TCA and TCE mixture is employed to investigate the numerical model and examine the importance of accounting for the occuring changes in the organic phase activity coefficients.

Model development

Multicomponent equilibrium aqueous solubility

Consider a single component NAPL at equilibrium with water in a closed system. Some NAPL molecules are dissolved in the aqueous phase and some water molecules are dissolved in the nonaqueous (organic) phase. However, due to the hydrophobic nature of the NAPL molecules, they do not dissolve easily in water (Schwarzenbach and others 1993). Figure 1 illustrates the dissolving activities of a single component NAPL and water, where the solid black circles represent NAPL molecules and the open white circles represent water molecules. The solubility of a single component NAPL in terms of mole fractions can be described by (Banerjee 1984)

$$X_s^w = \frac{X_s^\circ \gamma_s^\circ}{\gamma_s^w} \tag{1}$$

where X is the mole fraction of the slightly soluble species in the appropriate phase, γ is the activity coefficient; superscripts $\circ$ and w represent nonaqueous and aqueous phase, respectively, and subscript s indicates pure, single-component NAPL. The effect of water molecules dissolved into the nonaqueous phase is customarily neglected, and consequently the mole fraction of the contaminant in the nonaqueous phase is approximately equal to one. By assuming that the nonaqueous phase of a single component NAPL is at an ideal state with activity coefficient equal to one, the preceding equation can be reduced to

$$X_s^w = \frac{1}{\gamma_s^w} \tag{2}$$

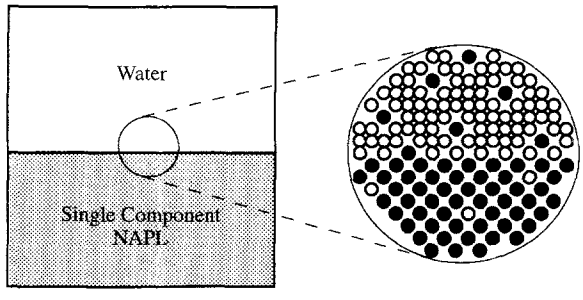

Fig. 1 Schematic illustration of single component NAPL dissolution

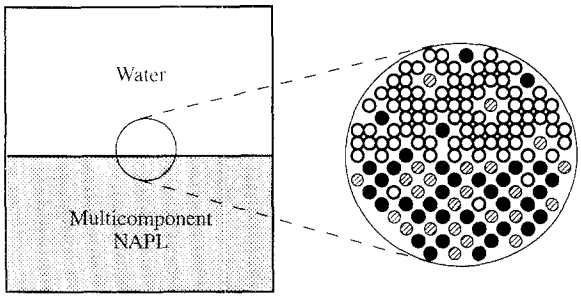

Fig. 2 Schematic illustration of multicomponent NAPL dissolution

The activities of a multicomponent system are illustrated in Fig. 2, where the solid black circles and open striped circles represent molecules of two different components, and the open white circles represent water molecules. The solubility of each component in terms of mole fractions is given by

$$X_p^w = \frac{X_p^\circ \gamma_p^\circ(X_p^\circ)}{\gamma_p^w(X_p^\circ)} \tag{3}$$

where the subscript p is the component indicator. It should be noted that the activity coefficients are dependent on the mole fraction of component p in the nonaqueous phase.

By dividing the preceding multicomponent solubility Eq. 3 with the pure, single-component reference solubility Eq. 2, yields a mole fraction ratio of the dissolving component p with respect to the mole fraction solubility of the pure component p. This dimensionless ratio is also equal to the concentration ratio of the equilibrium aqueous solubility of component p to its pure component solubility

$$\frac{X_p^w}{X_{s_p}^w} = \frac{C_p^w}{C_{s_p}} = \frac{X_p^\circ \gamma_p^\circ(X_p^\circ)\gamma_{s_p}^w}{\gamma_p^w(X_p^\circ)} \tag{4}$$

where C_p^w is the equilibrium aqueous solubility of component p, and C_{s_p}, is the pure, single-component saturation concentration of component p.

In view of Eq. 2, it is evident that the aqueous-phase activity coefficient is inversely proportional to the mole fraction of the NAPL. However, the majority of dissolved organic molecules present in groundwater have low solubility and they are not expected to react chemically with water; consequently, they are separated by large distances without hindering one another. For example, if *n*-octanol is used as the organic solvent, at equilibrium, there will only be about eight octanol molecules for every 100,000 water molecules in the aqueous phase (Schwarzenbach and others 1993). Therefore, it can be assumed that interactions among NAPL molecules in the aqueous phase are small, or $\gamma_{s_p}^w \simeq \gamma_p^w$, and Eq. 4 can be reduced to

$$C_p^w = C_{s_p} X_p^\circ \gamma_p^\circ(X_p^\circ) \tag{5}$$

The experimental studies conducted by Banerjee (1984) suggest that the nonaqueous phase activity coefficients of ideal state liquid mixtures are unaffected by the presence of cosolutes ($\gamma_p^\circ \simeq 1$). Therefore, for this special case, Eq. 5 simply reduces to Raoult's law

$$C_p^w = C_{s_p} X_p^\circ \tag{6}$$

Equations 5 and 6 represent two different approaches of equilibrium aqueous solubility estimation. Whenever possible, Eq. 5 should be used to account for the necessary correction in the activity of the liquids. The nonaqueous phase activity coefficient of each component in Equation 5 can be calculated using the group-contribution numerical code UNIFAC (Fredenslund and others 1977).

Model formulation

The transient contaminant transport from a dissolving multicomponent NAPL pool denser than water in a three-dimensional homogeneous porous medium under steady-state uniform flow conditions with the assumption that each component is sorbing under local equilibrium conditions, is governed by

$$R_p \frac{\partial C_p(t,x,y,z)}{\partial t} = D_{x_p} \frac{\partial^2 C_p(t,x,y,z)}{\partial x^2} + D_{y_p} \frac{\partial^2 C_p(t,x,y,z)}{\partial y^2} + D_{z_p} \frac{\partial^2 C_p(t,x,y,z)}{\partial z^2} - U_x \frac{\partial C_p(t,x,y,z)}{\partial x} - \lambda_p R_p C_p(t,x,y,z) \tag{7}$$

where $C(t,x,y,z)$ is the liquid phase solute concentration; U_x is the average interstitial fluid velocity; x, y, and z are the spatial coordinates in the longitudinal, lateral, and vertical directions, respectively; t is time; R is the dimensionless retardation factor for linear, reversible, instantaneous sorption; D_x, D_y, and D_z are the longitudinal, lateral, and vertical hydrodynamic dispersion coefficients, respectively; and λ is a first-order decay constant.

Assuming that a NAPL pool exists at the bottom of the aquifer and the thickness of the pool is insignificant relative to the thickness of the aquifer, the dissolution process is described by the following mass transfer relationship, applicable at the NAPL–water interface (Chrysikopoulos and others 1994)

$$-\mathscr{D}_{e_p} \frac{\partial C_p(t,x,y,0)}{\partial z} = k_p(t,x,y)[C_p^w(t) - C_p(t,x,y,\infty)] \tag{8}$$

where $\mathscr{D}_{e_p} = \mathscr{D}_p/\tau^*$ is the effective molecular diffusion coefficient of component p; $\mathscr{D}_p$ is the molecular diffusion coefficient; τ^* is the tortuosity ($\tau^* \geq 1$) (Carman 1937); $k_p(t,x,y)$ is the local mass transfer coefficient dependent on time and location at the NAPL–water interface; $C_p^w(t)$ is the equilibrium aqueous solubility, which is time dependent because the mole fraction of each component is changing as the NAPL dissolves into the aqueous phase.

Using proper initial and boundary conditions, Eq. 7 can be solved for NAPL pools of different shapes. Here, only a rectangular-shaped stagnant NAPL pool is examined, and the appropriate initial and boundary conditions for this system are (Chrysikopoulos 1995)

$$C_p(0,x,y,z) = 0 \tag{9}$$

$$C_p(t, \pm\infty, y, z) = 0 \tag{10}$$

$$C_p(t, x, \pm\infty, z) = 0 \tag{11}$$

$$\mathscr{D}_{e_p} \frac{\partial C_p(t, x, y, 0)}{\partial z} = \begin{cases} -k_p(t, x, y) C_p^w(t) & l_x < x < l_x + l_x \\ & l_y < y < l_y + l_y \\ 0 & \text{Otherwise} \end{cases} \tag{12}$$

$$C_p(t, x, y, \infty) = 0 \tag{13}$$

where l_x and l_y indicate the x and y Cartesian coordinates of the pool origin, respectively; l_x and l_y are the pool dimensions in x and y directions, respectively; $C_p(t, x, y, \infty) = 0$ corresponds to the contaminant concentration outside the boundary layer; $C_p^w(t)$ is given by Eq. 5 for nonideal or by Eq. 6 for ideal state liquid mixture and $\gamma_p^\circ(X_p^\circ)$ is obtained from UNIFAC, whereas the mole fraction $X_p^\circ(t)$ of component p at time t in both Eqs. 5 and 6 is defined as

$$X_p^\circ(t) = \frac{M_p(t)}{\sum_{p=1}^{P} M_p(t)} \qquad (p = 1, 2, \ldots, P) \tag{14}$$

where P is the total number of components in the nonaqueous phase; $M_p(t)$ is the number of moles of component p present in the nonaqueous phase at time t, and is defined by

$$M_p(t) = M_p' - \sum_{m=1}^{m_f} \frac{k_p^* \, C_p^w(m\Delta t) \, l_x l_y \Delta t \, X_p^\circ(m\Delta t)}{(\text{mol wt})_p} \qquad (t \geq \Delta t) \tag{15}$$

where M_p' is the initial number of moles of component p in the nonaqueous phase; Δt is the time step; m is a summation index; m_f is an integer indicating the total number of time steps, and is defined as

$$m_f = I\left(\frac{t}{\Delta t}\right) \qquad (m_f = 1, 2, 3 \ldots) \tag{16}$$

where $I(\ )$ is an integer mode arithmetic operator truncating the numeric argument by chopping off any fractional part; and $k_p^* = k_p(t, x, y)$ represents the special case where the local mass transfer coefficient can be replaced by an average (or overall) mass transfer coefficient, because $k_p(t, x, y)$ is case specific and can only be obtained experimentally.

Numerical solution

The finite-difference approximation employed in this work requires the discretization of the governing partial differential equation (Eq. 7). By using the implicit (or backward) finite-difference method, where the space derivative is evaluated at the advanced time level $(n + 1)$ with equal distances between the nodes in the x, y, and z spatial coordinates Δx, Δy, and Δz, respectively, the discretized governing equation is (Wang and Anderson 1982).

$$\begin{aligned} \frac{R}{\Delta t}(C_{i,j,k}^{n+1} - C_{i,j,k}^n) = {} & \frac{D_x}{(\Delta x)^2}(C_{i+1,j,k}^{n+1} - 2C_{i,j,k}^{n+1} + C_{i-1,j,k}^{n+1}) \\ & + \frac{D_y}{(\Delta y)^2}(C_{i,j+1,k}^{n+1} - 2C_{i,j,k}^{n+1} + C_{i,j-1,k}^{n+1}) \\ & + \frac{D_z}{(\Delta z)^2}(C_{i,j,k+1}^{n+1} - 2C_{i,j,k}^{n+1} + C_{i,j,k-1}^{n+1}) \\ & - \frac{U_x}{2\Delta x}(C_{i+1,j,k}^{n+1} - C_{i-1,j,k}^{n+1}) - \lambda R C_{i,j,k}^{n+1} \end{aligned} \tag{17}$$

where i, j, and k are the corresponding nodes in x, y, and z directions, respectively. Collecting like terms in the preceding equation leads to

$$\begin{aligned} \vartheta C_{i,j,k}^n = {} & \alpha C_{i,j,k}^{n+1} + \zeta C_{i-1,j,k}^{n+1} + \beta C_{i+1,j,k}^{n+1} + \kappa C_{i,j-1,k}^{n+1} \\ & + \kappa C_{i,j+1,k}^{n+1} + \mu C_{i,j,k-1}^{n+1} + \mu C_{i,j,k+1}^{n+1} \end{aligned} \tag{18}$$

where

$$\alpha = -\left(\frac{R}{\Delta t} + \frac{2D_x}{(\Delta x)^2} + \frac{2D_y}{(\Delta y)^2} + \frac{2D_z}{(\Delta z)^2} + \lambda R\right) \tag{19}$$

$$\beta = \frac{D_x}{(\Delta x)^2} - \frac{U_x}{2\Delta x} \tag{20}$$

$$\vartheta = -\frac{R}{\Delta t} \tag{21}$$

$$\kappa = \frac{D_y}{(\Delta y)^2} \tag{22}$$

$$\mu = \frac{D_z}{(\Delta z)^2} \tag{23}$$

$$\zeta = \frac{D_x}{(\Delta x)^2} + \frac{U_x}{2\Delta x} \tag{24}$$

Finally, the flux boundary conditions are incorporated into the numerical model by using the following second-order accurate one-sided approximation (Strikwerda 1989)

$$\frac{\partial C(t, x, y, 0)}{\partial z} \approx \frac{-3C_{i,j,1}^n + 4C_{i,j,2}^n - C_{i,j,3}^n}{2\Delta z} \tag{25}$$

Equation 18 can be expanded to any number of grid points; however, for every additional grid point the system increases by one unknown and one equation. The resulting matrix is a band diagonal system of equations. The concentrations at the next advanced time level $(n + 1)$ can be obtained efficiently by using the subroutines *banmul*, *bandec*, and *banbks* presented by Press and others (1992).

Simulations and discussion

Consider a rectangular NAPL pool located at the bottom of a sandy aquifer with interfacial area $l_x \times l_y = 0.28 \times 0.18$ m^2, whose origin has coordinates $l_x = 0.22$ m and $l_y = 0.09$ m. The steady, unidirectional groundwater flow

Table 1 Parameter values for numerical simulations

Parameter	Value
C_s	4.5[a], 1.1[b] g l^{-1} (Miller and others 1990)
$\mathscr{D}_e$	2.33 × 10^{-6a}, 2.43 × 10^{-6b} m^2 h^{-1}
D_x	9.0 × 10^{-5} m^2 h^{-1}
D_y, D_z	2.33 × 10^{-6a}, 2.43 × 10^{-6b} m^2 h^{-1}
k^*	1.5 × 10^{-4a}, 1.95 × 10^{-4b} m h^{-1}
l_x, l_y	0.28, 0.18 m
l_x, l_y	0.22, 0.09 m
Mol wt	133.4[a], 131.5[b] g mol^{-1} (Whelan 1992)
M'	0.5[a], 0.5[b] mol
η_w	0.8904 cp at 25°C (Lyman and others 1982)
P	2
R	1.1[a], 1.87[b] (Whelan 1992)
U_x	3.125 × 10^{-3} m h^{-1}
λ	0.0 h^{-1}
τ^*	1.43

[a] Data for TCA
[b] Data for TCE

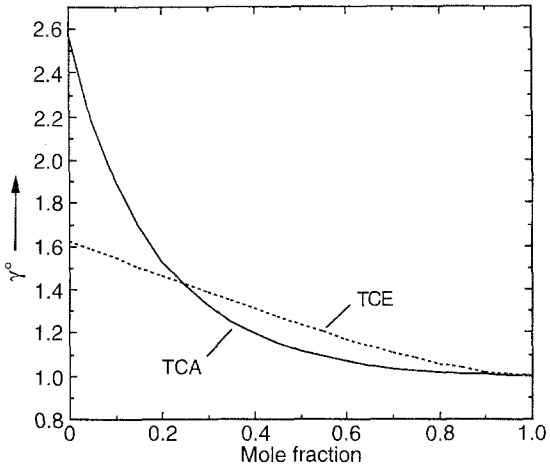

Fig. 3 UNIFAC predictions of organic phase activity coefficients for TCE and TCA as a function of mole fraction

Table 2 Volume increments for LeBas method (Lyman and others 1982).

Atom	Increment (cm^3 mol^{-1})
C	14.8
Cl	24.6
H	3.7
O	7.4

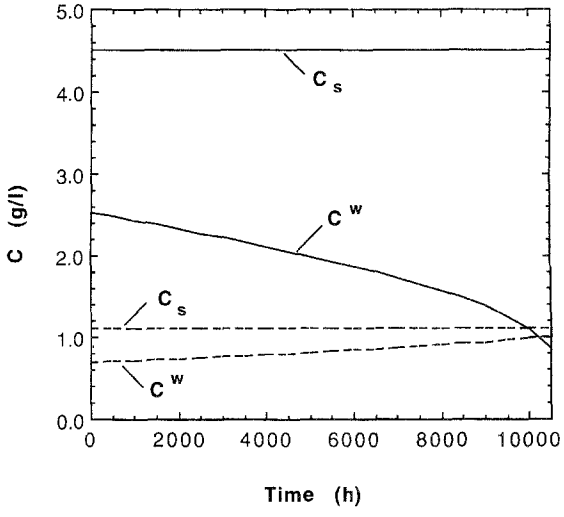

Fig. 4 Comparison between the equilibrium aqueous solubility and the pure single component solubility as a function of time for TCA (solid lines) and TCE (dashed lines)

is along the x coordinate. The NAPL pool consists of two well-mixed equimolar components, namely TCA and TCE. To predict concentrations of the two dissolving components in the vicinity of the pool, the numerical model presented in the previous section is used. All model parameters used for the simulations are listed in Table 1. A TCA/TCE mixture is chosen because a preliminary experimental study on this particular mixture has been conducted by Whelan (1992), so realistic values for the retardation factor (R) in silica sand and the mass transfer coefficient (k^*) for each component can be used.

The molecular diffusion coefficient, $\mathscr{D}_p$ (square meters per hour), of each component p, is estimated by the Hayduk and Laudie (1974) relationship

$$\mathscr{D}_p = \frac{4.77 \times 10^{-5}}{\eta_w^{1.14} V_p^{0.589}} \tag{26}$$

where η_w (centipoise) is the viscosity of water at the desired temperature [at 25°C η_w = 0.8904 cp (Lyman and others 1982)], and V_p (cubic centimeters per mole) is the molar volume for the particular component. The molar volume is calculated using the LeBas method (Lyman and others

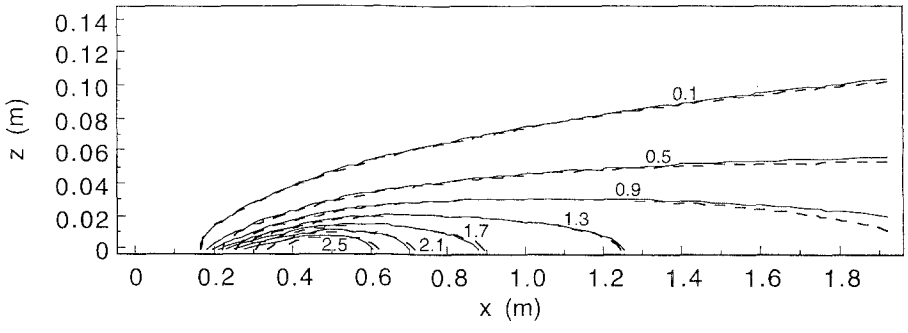

Fig. 5 Comparison between concentration contours in the x, z plane obtained by the analytical solution presented by Chrysikopoulos (1995) (dashed lines) and the finite-difference scheme (solid lines) for a single component NAPL pool [$C^w(t)$ = C_s = 4.5 g/l, y = 0.18 m]

1982). This method sums the volume increments of every individual atom in the molecule and subtracts any volume correction for the shape or structure of the molecule. A list of LeBas volume increments associated with TCA and TCE is presented in Table 2. Following this procedure, TCA ($C_2H_3Cl_3$) has a LeBas molar volume of 114.5 cm^3 mol^{-1} [(2 × 14.8) + (3 × 3.7) + (3 × 24.6)] and TCE (C_2HCl_3) has a LeBas molar volume of 107.1 cm^3/mol^{-1} [(2 × 14.8) + 3.7 + (3 × 24.6)]. Substituting these values into Eq. 26, the estimated molecular diffusion coefficients are 3.33 × 10^{-6} m^2 h^{-1} and 3.47 × 10^{-6} m^2 h^{-1} for TCA and TCE, respectively. Assuming that the sandy model aquifer has a tortuosity of $\tau^* = 1.43$ (de Marsily 1986), the effective molecular diffusion coefficient ($\mathscr{D}_{e_p} = \mathscr{D}_p/\tau^*$) for TCA is 2.33 × 10^{-6} m^2 h^{-1} and for TCE is 2.43 × 10^{-6} m^2 h^{-1}.

The nonaqueous phase activity coefficients of the organics present in the multicomponent pool are obtained by using the program UNIFAC. Figure 3 shows the relationship between the organic phase activity coefficient as a function of mole fraction for TCA and TCE, as estimated by UNIFAC. This figure indicates that the solution nonideality increases as the mole fraction of each component in the mixture decreases. Appropriate mathematical expressions representing the UNIFAC relationships presented in Fig. 3 are incorporated into the numerical model for activity coefficient determination.

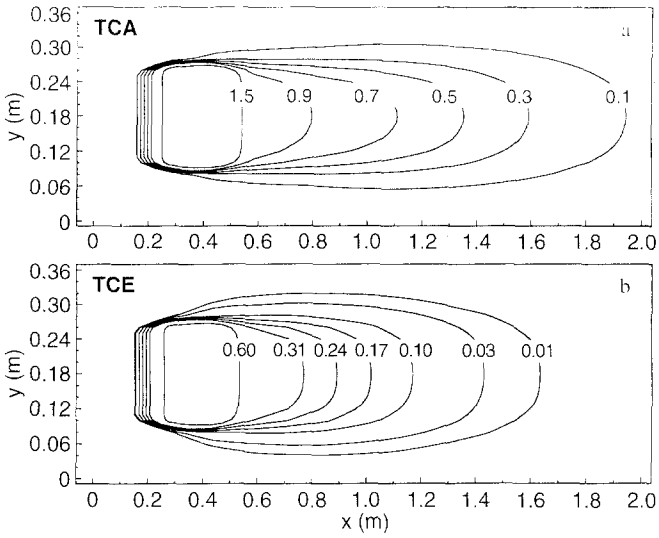

Fig. 6 Concentration contour plots of (**a**) TCA and (**b**) TCE (grams per liter) in the x, y plane at 500 h ($z = 0.0$ m)

Figure 4 shows the pure component solubilities and the equilibrium aqueous solubilities for TCA and TCE. Since the pool is assumed to maintain its shape with time, the simulation cannot run until complete disappearance of the contaminant. However, Fig. 4 indicates that the TCA equilibrium aqueous solubility approaches zero with in-

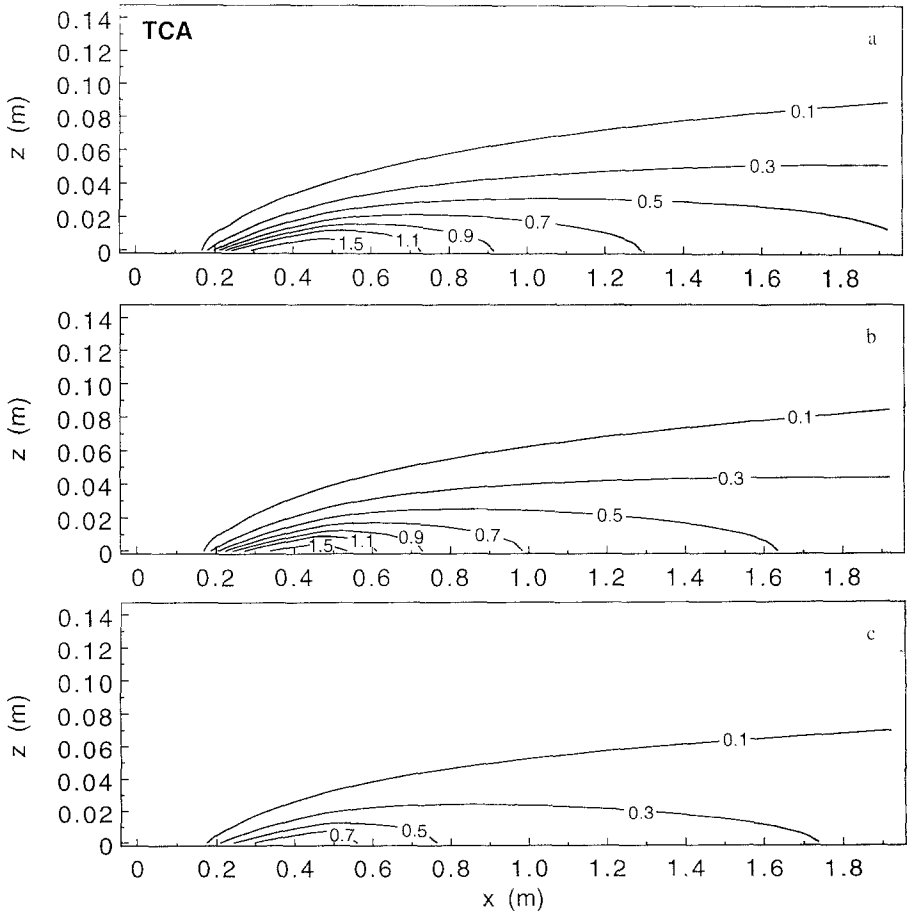

Fig. 7 Contour plots of TCA concentration (grams per liter) in the x, z plane at (**a**) 1000, (**b**) 5000, and (**c**) 10,000 h ($y = 0.18$ m)

creasing time, whereas that for TCE approaches its pure component solubility. The TCA equilibrium aqueous solubility decreases with increasing time because TCA has a higher solubility (4.5 g l^{-1}) than TCE (1.1 g l^{-1}) (Miller and others 1990) and over time more TCA is dissolved, leading to a lower TCA mole fraction.

In order to verify the finite-difference scheme presented in the previous section, concentration contour plots in the x, z plane obtained by the numerical model are compared with corresponding contours generated by the analytical three-dimensional solution derived by Chrysikopoulos (1995) for the case of a single component TCA pool at $t = 10{,}000$ h. The model predictions from the two solutions are in very good agreement and are shown in Fig. 5. With confidence in the numerical model, we can proceed to simulate the more complex case of contaminant transport from multicomponent NAPL pool dissolutions.

Figure 6 shows the concentration contours in the x, y plane at 500 h since the initiation of the dissolution process for (a) TCA and (b) TCE, respectively. Figures 7 and 8 present concentration contours in the x, z plane at (a) 1000, (b) 5000, and (c) 10,000 hours since the initiation of the dissolution process for TCA and TCE, respectively. Figs. 7a–c indicate a decrease in TCA plume concentration levels with increasing time; whereas Figs. 8a–c indicate a steady increase in TCE plume size and concentration levels with increasing time. According to Fig. 4, the equilibrium aqueous solubility for TCA decreases with time; therefore, the concentration contours are also expected to decrease with time. Conversely, the concentration contours for TCE are expected to increase with time. The results of Figs. 7 and 8 are in good agreement with the equilibrium aqueous solubility relationships presented in Fig. 4.

Concentration breakthrough curves at a point within the model aquifer with coordinates $x = 0.72$ m, $y = 0.18$ m, and $z = 0.005$ m for TCA are illustrated in Fig. 9a and for TCE in Fig. 9b. The solid lines represent NAPL concentration with the equilibrium aqueous solubility calculated using Eq. 5, thus accounting for the necessary correction in the activity of the liquids as predicted by UNIFAC. The dashed lines represent NAPL concentration with the equilibrium aqueous solubility calculated using Eq. 6, where the equilibrium aqueous solubility solely depends on the mole fraction of a single component ($\gamma^\circ = 1$). These breakthrough curves indicate the important result that dissolved contaminant concentrations may be quite underestimated if the nonaqueous phase activity coefficient is neglected in calculating the equilibrium aqueous solubility.

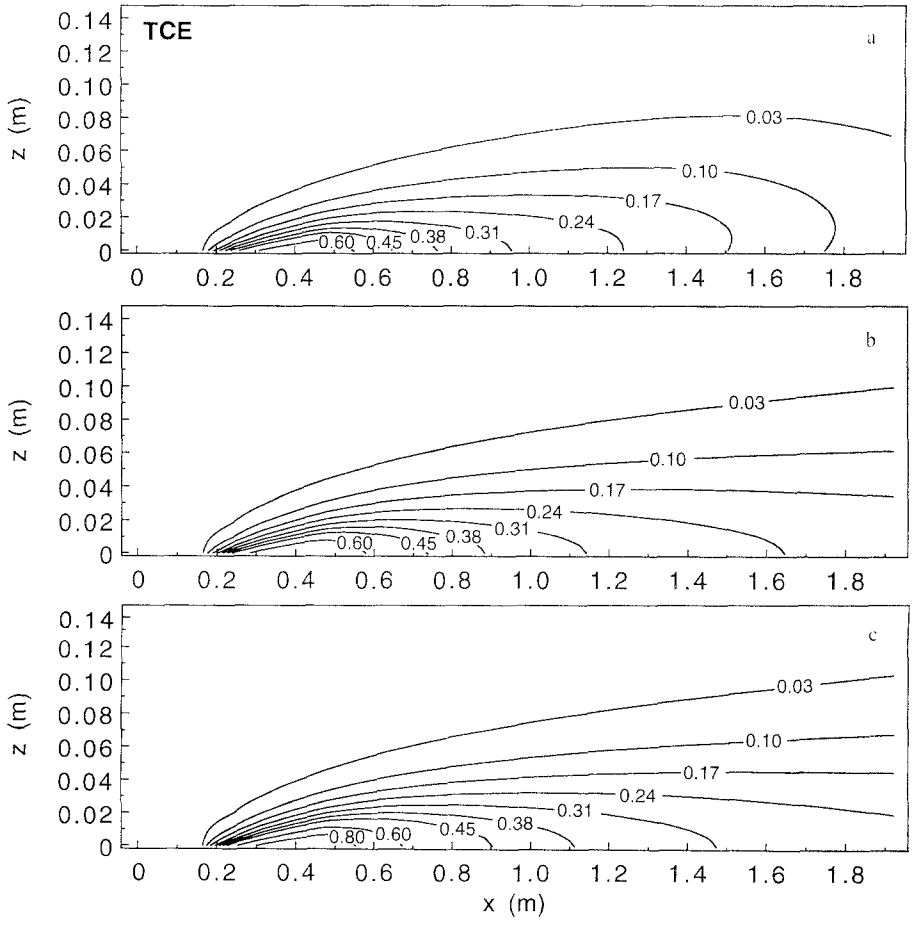

Fig. 8 Contour plots of TCE concentration (grams per liter) in the x, z plane at (**a**) 1000, (**b**) 5000, and (**c**) 10,000 h ($y = 0.18$ m)

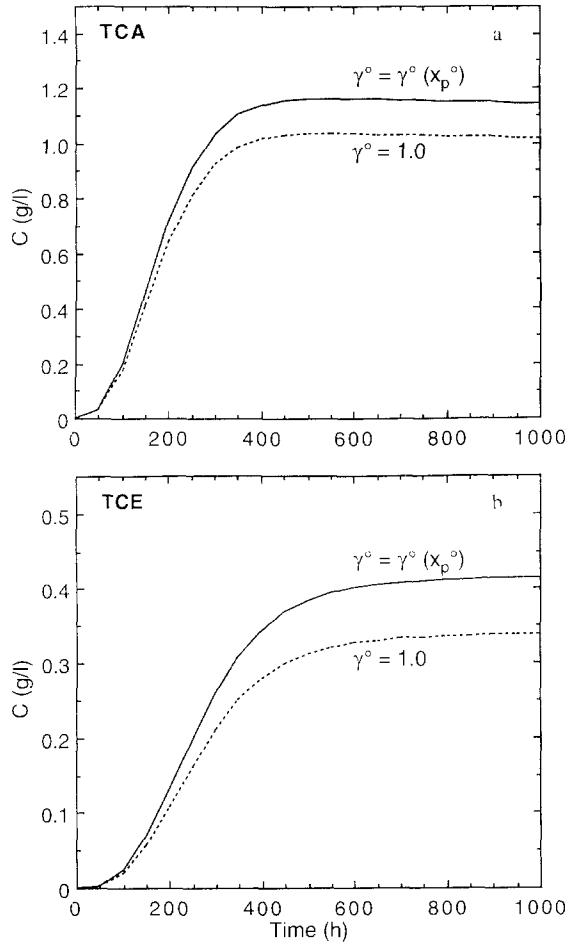

Fig. 9 Comparison between breakthrough curves obtained with the equilibrium aqueous solubility calculated using Eq. 5 (solid lines) and Eq. (6) (dashed lines) for (**a**) TCA and (**b**) TCE ($x = 0.72$ m, $y = 0.18$ m, $z = 0.005$ m)

Summary and conclusions

A finite-difference numerical model is presented to simulate multicomponent transport resulting from the dissolution of a stagnant NAPL pool at the bottom of a three-dimensional, homogeneous porous formation. The model assumes that contaminant dissolution is mass-transfer limited and accounts for changes in the equilibrium aqueous concentration for each component with time, by calculating the time-dependent mole fractions. The required nonaqueous phase activity coefficients are obtained by the numerical code UNIFAC. Neglecting the changes in the nonaqueous phase activity coefficient, may lead to a significant underestimation in dissolved aqueous phase concentrations as demonstrated for the case of a NAPL pool consisting of a mixture of TCA and TCE. The model presented in this work can be used to predict the transport and fate of multicomponent NAPL pool dissolutions in groundwater systems and, furthermore, to interpret actual field data sampled at contamination sites associated with NAPL pool dissolutions. Some weaknesses of the model presented are the required extensive computational memory and the need for numerous physical parameter values for each component present in a particular pool mixture.

Acknowledgements The authors thank Assem Abdel-Salam and Evangelos Voudrias for their contributions to this study. This work was sponsored by the U.S. Environmental Protection Agency. However, the manuscript has not been subjected to the Agency's peer and administrative review and therefore does not necessarily reflect the views of the Agency and no official endorsement should be inferred.

Notation

C	liquid phase solute concentration (solute mass/liquid volume) (M L^{-3})
C_s	single component aqueous saturation concentration (solubility) (M L^{-3})
C^w	equilibrium aqueous solubility (M L^{-3})
$\mathscr{D}$	molecular diffusion coefficient (L^2 t^{-1})
$\mathscr{D}_e$	effective molecular diffusion coefficient (L^2 t^{-1})
D_x	longitudinal hydrodynamic dispersion coefficient (L^2 t^{-1})
D_y	lateral hydrodynamic dispersion coefficient (L^2 t^{-1})
D_z	hydrodynamic dispersion coefficient in the vertical direction (L^2 t^{-1})
$I(\ )$	integer mode arithmetic operator
k	local mass transfer coefficient (L t^{-1})
k^*	average mass transfer coefficient (L t^{-1})
L	length
l_x, l_y	pool dimensions in x and y directions (L)
l_{x°, l_{y°	x and y Cartesian coordinates of the pool origin (L)
M	number of moles remaining in a pool (moles)
M'	initial number of moles (moles)
n	finite-difference scheme time level
R	retardation factor (dimensionless)
t	time (t)
U_x	average interstitial velocity (L t^{-1})
x, y, z	spatial Cartesian coordinates (L)
X	dimensionless mole fraction
γ	dimensionless activity coefficient
η_w	viscosity of water (=0.8904 cp at 25°C)
λ	decay coefficient (t^{-1})
τ^*	tortuosity (≥ 1)
Subscripts	
i, j, k	finite-difference scheme grid indicators
p	component number indicator
P	total number of components
s	pure single component
Superscripts	
$\circ$	nonaqueous phase
w	aqueous phase

References

Adenekan AE, Patzek TW, and Pruess K (1993) Modeling of multiphase transport of multicomponent organic contaminants and heat in the subsurface: Numerical model formulation. Water Resour Res 29(11):3727–3740

Anderson MR, Johnson RL, and Pankow JF (1992a) Dissolution of dense chlorinated solvents into groundwater, 1, Dissolution from a well-defined residual source. Ground Water 30(2):250–256

Anderson MR, Johnson RL, and Pankow JF (1992b) Dissolution of dense chlorinated solvents into groundwater, 3, Modeling contaminant plumes from fingers and pools of solvent. Environ Sci Technol 26(5):901–908

Banerjee S (1984) Solubility of organic mixtures in water. Environ Sci Technol 18(8):587–591

Borden RC and Piwoni MD (1992) Hydrocarbon dissolution and transport: a comparison of equilibrium and kinetic models. J Contam Hydrol 10:309–323

Carman PC (1937) Fluid flow through granular beds. Trans Inst Chem Eng London 15:150–156

Chrysikopoulos CV (1995) Three-dimensional analytical models of contaminant transport from nonaqueous phase liquid pool dissolution in saturated subsurface formations. Water Resour Res 31(4):1137–1145

Chrysikopoulos CV, Voudrias EA, and Fyrillas MM (1994) Modeling of contaminant transport resulting from dissolution of nonaqueous phase liquid pools in saturated porous media. Transport Porous Media 16(2):125–145

de Marsily G (1986) Quantitative hydrogeology, groundwater hydrology for engineers. Orlando, Florida: Academic Press. 440 pp

Fredenslund A, Gmehling J, and Rasmussen P (1977) Vapor–liquid equilibria using UNIFAC. New York: Elsevier. 380 pp

Geller JT (1990) Dissolution of non-aqueous phase organic liquids in porous media. PhD dissertation. University of California-Berkeley

Geller JT and Hunt JR (1993) Mass transfer from nonaqueous phase organic liquids in water-saturated porous media. Water Resour Res 29(4):833–845

Hayduk W and Laudie H (1974) Prediction of diffusion coefficients for nonelectrolytes in dilute aqueous solutions. AIChE J 20(3): 611–615

Hunt JR, Sitar N, and Udell KS (1988) Nonaqueous phase liquid transport and cleanup, 1, Analysis of mechanisms. Water Resour Res 28(4):1247–1258

Johnson RL and Pankow JF (1992) Dissolution of dense chlorinated solvents into groundwater, 2, Source functions for pools of solvent. Environ Sci Technol 26(5):896–901

Lyman WJ, Reehl WF, and Rosenblatt DH (1982) Handbook of chemical property estimation methods. New York: McGraw Hill. 977 pp

Miller CT, Poirier-McNeill MM, and Mayer AS (1990) Dissolution of trapped nonaqueous phase liquids: Mass transfer characteristics. Water Resour Res. 26(11):2783–2796.

Pinder GF and Abriola LM (1986) On the simulation of nonaqueous phase organic compounds in the subsurface. Water Resour Res 22(9):109S–119S

Powers SE, Loureiro CO, Abriola LM, and Weber WJ Jr (1991) Theoretical study of the significance of nonequilibrium dissolution of nonaqueous phase liquids in subsurface systems. Water Resour Res 27(4):463–477

Powers SE, Abriola LM, and Weber WJ Jr (1992) An experimental investigation of nonaqueous phase liquid dissolution in saturated subsurface systems: steady state mass transfer rates. Water Resour Res 28(10):2691–2705

Press WH, Flannery BP, Teukolsky SA, and Vetterling WT (1992) Numerical recipes: The art of scientific computing, 2nd ed. Cambridge: Cambridge University Press. 963 pp

Schwarzenbach RP, Gschwend PM, and Imboden DM (1993) Environmental organic chemistry. New York: Wiley. 681 pp

Strikwerda JC (1989) Finite difference schemes and partial differential equations. Pacific Grove, California: Wadsworth & Brooks/Cole. 386 pp

Stumm W and Morgan JJ (1981) Aquatic chemistry, 2nd ed. New York: Wiley. 780 pp

Voudrias EA and Yeh MF (1994) Dissolution of a toluene pool under constant and variable hydraulic gradients with implications for aquifer remediation. Groundwater 32(2):305–311

Wang HF and Anderson MP (1982) Introduction to groundwater modeling. New York: W.H. Freeman. 237 pp

Whelan MP (1992) Dissolution of non-aqueous phase liquid pools in saturated porous media. Master's thesis. Atlanta, Georgia, USA Georgia Institute of Technology